Journal of Energy Storage 154 (2026) 121164

Contents lists available at ScienceDirect

Journal of Energy Storage

journal homepage: www.elsevier.com/locate/est

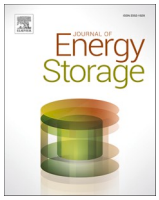

Research papers

Exploring the potential of a potash by-product for thermochemical heat storage

V. Mamani [a], A. Gutiérrez [b], A.I. Fernández [c,*], S. Ushak [d]

[a] Department of Thermal Energy Storage, Iberian Centre for Research in Energy Storage, CIIAE. Avda de las letras, s/n, Campus University of Extremadura, 10003, Cáceres, Spain
[b] German Aerospace Center – DLR e. V., Institute of Engineering Thermodynamics, Pfaffenwaldring 38, 70569 Stuttgart, Germany
[c] DIOPMA Research Group. Dept of Materials Science and Physical Chemistry, Universitat de Barcelona, Martí i Franqués 1, 08028 Barcelona, Spain
[d] Center for Advanced Study of Lithium and Industrial Minerals (CELiMIN), Departamento de Ingeniería Química y Procesos de Minerales, Universidad de Antofagasta, Campus Coloso, Av. Universidad de Antofagasta, 02800, Antofagasta, Chile.

ARTICLE INFO

Keywords:
Thermochemical energy storage
Carnallite
By-products
Seasonal heat storage
Reversible reaction

ABSTRACT

Thermochemical energy storage is an effective method for seasonal heat storage applications, as it stores energy on a long-term basis. This process captures excess heat generated during the summer, whether from solar energy or surplus heat from supply chains, and utilizes it during the winter months. However, the process relies on chemical reactions, which pose various technical challenges. Additionally, it requires a significant amount of materials, leading to increased system costs. In this study, we propose to investigate potassium carnallite as a low-cost thermochemical material (TCM). This material is derived from potash saline deposits located in northeastern Spain. Characterization through chemical analysis revealed that it comprises 86.0% $KCl{\cdot}MgCl_2{\cdot}6H_2O$, with NaCl as the main impurity at a concentration of 10%. The dehydration and hydration reactions analyzed involve the loss and retention of 4 molecules of H_2O. Importantly, there is no evidence that the hydrolysis decomposition of the material affects the reversibility of these reactions. The study demonstrated a good reversibility of the reaction, with a yield of 81.73%, which decreased to 78.83% by the tenth cycle. These cycles simulate 10 years of seasonal use under specific conditions ($P_{Hy} = 1.3$ kPa, $T_{Hy} = 40$ °C, $P_{De} = 4.0$ kPa, and $T_{De} = 110$ °C). Notably, natural carnallite exhibited 20% higher reversibility compared to synthetic carnallite. However, it was found to be 14% less reversible during the first cycle and 8.4% less reversible by the tenth cycle compared to another carnallite material studied under the same conditions previously. This difference in reversibility may be attributed to variations in the impurity content of both materials, where a higher concentration of NaCl in carnallite may act as a chemical spacing, facilitating water vapor mass transfer and consequently improving cycling stability. We measured an energy density of 0.892 GJ/m^3 during the tenth hydration cycle, indicating that the winter energy needs of a household can be met using 9.0 m^3 of thermochemical material. These findings suggest that by-products from mining, such as carnallite, are promising candidates for seasonal heat storage applications. However, improvements in the material are needed to increase the energy density at large scale, which would consequently reduce the volume of material required for the application using a reactor system.

1. Introduction

Thermal energy constitutes the most significant portion of global energy use, accounting for approximately 50% of the world's energy consumption. Approximately half of the consumed heat is utilized in industry, while the other half is used for domestic purposes. Together, these account for around 25% of final energy consumption, which totals about $8{\cdot}10^{18}$ J/year, according to Eurostat [1].

The current necessity to decarbonize the European economy and implement the European Green Deal [2] requires efficient methods for storing and upgrading thermal energy. This is essential for tapping into the significant energy-saving potential of available waste heat and the increasing capacity of renewable energy sources [3]. Consequently, developing effective ways to transform and store thermal energy has

* Corresponding author.
E-mail address: ana_inesfernandez@ub.edu (A.I. Fernández).

https://doi.org/10.1016/j.est.2026.121164
Received 3 June 2025; Received in revised form 29 January 2026; Accepted 16 February 2026
Available online 25 February 2026

become a pressing priority for the European Union.

One of the most promising technologies for compact and efficient long-term thermal energy storage is Thermochemical Energy Storage (TCES). This technology is based on using reversible chemical reactions that have high heat effects, utilizing abundant and benign thermochemical materials [4,5].

The most critical aspect of (TCES) systems, compared to sensible or latent heat storage, is that they require higher investment costs; however, a recent techno-economic analysis by Yang et al. [6] indicates that, despite TCES excels in technical aspects over other thermal energy storage (TES) technologies, it will become competitive once the cost of materials is reduced. Thermochemical materials represent a significant portion of these total investment costs, often exceeding 30%, and this cost tends to increase as the system scales up [7]. Therefore, it is essential to identify and explore low-cost, non-critical materials that can effectively serve as storage media for TCES.

Recent advancements in resource recovery technology have made the extraction of minerals and metals from industrial waste and seawater desalination brine more cost-competitive compared to commercial inorganic materials [8–10]. From this, carnallite is a hydrated evaporite salt that forms during the natural evaporation of seawater. It is found alongside other potassium and magnesium compounds in evaporite deposits. Being easily accessible and often produced as a by-product of potassium mining, carnallite is both inexpensive and sustainable.

Salt hydrates have become the preferred materials for the emerging TCES systems operating at low temperatures [7] ($T < 200$ °C). Salt hydrates can be dehydrated by a surplus of heat, thus charging the system (Fig. 1). In the charged state, heat is stored as the chemical potential of the dehydrated salt relative to the reaction with water vapor. When the stored heat is needed during the wintertime, one can carry out the reverse reaction at a useful temperature 30-80 °C by withdrawing heat from an ambient low-temperature source (e.g. T ~ 10 °C) to create water vapor pressure high enough (p ~ 1.3 kPa) to carry out the exothermic hydration [11] (Eq. (1)):

$$\text{Salt} + n\text{H}_2\text{O} \rightleftharpoons \text{Salt}\cdot n\text{H}_2\text{O} + \text{Heat} \quad (1)$$

Currently, the most widely used hydrated salts for TCES are single (chlorides, sulfates, bromides), both as pure compounds and in composites. However, only a few studies have been conducted on salt mixtures. Many of these materials can be obtained from seawater, as well as industrial waste materials (Table 1).

Carnallite, a low-cost industrial waste material, was first investigated as a thermochemical material by Gutierrez et al. [10,12]. While their primary focus was on high-temperature applications, they also identified carnallite as a potential material for low-temperature uses. This research was further developed by Mamani et al. [7], who studied an industrial waste material containing approximately 73.5% pure carnallite. The study found a good cyclability under seasonal conditions (dehydration at 110 °C/4.0 kPa and rehydration at 40 °C/1.3 kPa) (Eq. (2)), avoiding the material decomposition by temperature effect and the hydrolysis reaction of $MgCl_2{\cdot}2\,H_2O(s)$ (Eq. (3)). However, still an incomplete rehydration and a slow kinetic hydration were found after 10 cycles of reaction. This research is supported by additional research conducted by R. Hamze et al. [13]. In their theoretical and experimental study, they concluded that carnallite, when compared to other single and double salts, shows great promise for low-temperature thermochemical storage. It is a low-cost material with a high deliquescence humidity, making it significantly less sensitive to over-hydration and liquefaction. Additionally, carnallite can be easily dehydrated at just 100 °C. The rehydration process can be achieved at low water vapor pressures, resulting in a storage density of 1.52 kJ/cm^3.

$$\text{KCl}\cdot\text{MgCl}_2\cdot 6\,\text{H}_2\text{O}\,(s) \rightleftharpoons \text{KCl}\cdot\text{MgCl}_2\cdot 2\,\text{H}_2\text{O}(s) + 4\,\text{H}_2\text{O}(g) \quad (2)$$

$$\text{KCl}\cdot\text{MgCl}_2\cdot 2\,\text{H}_2\text{O}\,(s) \rightleftharpoons \text{KCl}\cdot\text{MgCl}_2(s) + 2\,\text{H}_2\text{O}(g) + \text{KMg}\,(\text{OH})\text{Cl}\,(s) + 2\,\text{HCl}\,(g) \quad (3)$$

Based on the current state of the art and the advantages of identifying low-cost materials for heat storage, this study aims to characterize a by-product from a potash deposit in Bages, located in the northeast of Spain. The material will undergo chemical characterization and be evaluated as a potential thermochemical storage material under seasonal conditions, compared with another source of carnallite as a by-product material and a synthetic $KCl{\cdot}MgCl_2{\cdot}6\,H_2O$.

2. Materials and methods

2.1. Material selection

Approximately 1 kg of natural carnallite was provided by ICL Iberia Súria and Sallent (Catalunya region, Spain) and obtained from natural potash deposits in Súria. The sample was homogenized by manual mixing and then subjected to drying at 40 °C for approximately 12 h to eliminate environmental humidity, due to the hygroscopic nature of the salt. The sample was designated as Carnallite B for the comprehensive study.

2.2. Chemical characterization

2.2.1. Chemical analysis

For the chemical analysis, 200 mg of Carnallite B was dissolved in 1% v/v HNO_3 until a concentration of 2 mg/mL was achieved to be analyzed using the ICP-OES (Inductively Coupled Plasma Atomic Emission

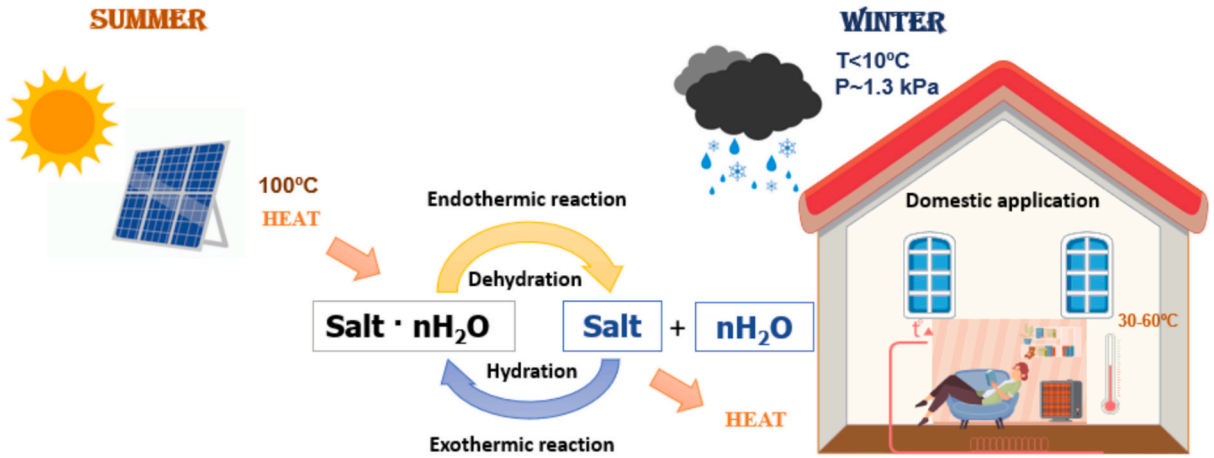

Fig. 1. Left: scheme of thermochemical reaction for heat storage. Right: Seasonal heat storage application for private households.

Table 1
The most widely used hydrated salts for TCES. Simple and double salts. Experimental and theoretical information (* related to studied industrial waste materials, ♣ theoretical information).

Hydrated salt		Operational conditions T_{De} (°C), P_{Hy} (mbar)		Energy Density (GJ/m^3)	Main findings	Ref.
Chlorides	* $CaCl_2$ $CaCl_2(s)$ /$CaCl_2 \cdot 2H_2O(s)$	180 °C	445 mbar	7.16	Good reversibility and cycling stability over 20 cycles.	[14]
	* $MgCl_2$ $MgCl_2(s)/MgCl_2 \cdot 6H_2O(s)$	150 °C	11.8 31.6 mbar	1.89–1.94	HCl by-product above 110–130 °C	[15]
	LiCl LiCl (s)/ LiCl·H_2O(s)	160–186 °C	—	1.9–2.5	LiCl·H_2O exhibits one of the highest energy densities	[16]
	* $SrCl_2$ $SrCl_2$ (s)/ $SrCl_2 \cdot 6H_2O(s)$	130 °C	14–16	2.4	Poor heat and mass transfer performance and low cyclic stability	[17]
Sulfates	* $MgSO_4$ $MgSO_4(s)$/ $MgSO_4 \cdot 7H_2O(s)$	150 °C	12.5–13	1.8–2.2	Heat release above 50 °C is not possible	[18]
	♣$CaSO_4$ $CaSO_4$ (s)/$CaSO_4 \cdot 2H_2O(s)$	89	—	1.4	Lower energy density, but its stability, abundance, and affordability	[19]
	♣$Al_2(SO_4)_3$ $Al_2(SO_4)_3.5H_2O(s)/Al_2(SO_4)_3.18H_2O(s)$	80–125 °C	—	2.16	Four endothermic stages and moderate energy density	[20]
Bromides	$SrBr_2$ $SrBr_2(s)$/ $SrBr_2 \cdot H_2O(s)$	80 °C	9.7–17.5	2.02	High cost	[21]
	LiBr LiBr(s)/ LiBr · $H_2O(s)$	95 °C	50	2.8	Highly corrosive to metals	[22]
Doble salts	* Lithium Carnallite $LiCl \cdot MgCl_2(s)/LiCl \cdot MgCl_2 \cdot 7H_2O(s)$	200 °C	—	—	Partial decomposition below 200 °C	[10]
	* Potassium Carnallite $KCl \cdot MgCl_2 \cdot 4H_2O(s)$/ $KCl \cdot MgCl_2 \cdot 6H_2O(s)$	110 °C	13	1.4	HCl by-product above 130 °C	[7]
	* Kainite $KCl \cdot MgSO_4(s)/KCl \cdot MgSO_4 \cdot 3H_2O(s)$	200 °C	—	—	Further research is needed	[23]
	* Bloedite, Astrakanite $Na_2SO_4 \cdot MgSO_4(s)$/ $Na_2SO_4 \cdot MgSO_4 \cdot 4H_2O(s)$	200 °C	—	1.3	The melting process occurs at $T = 671.2$ °C	[10,23]

Spectroscopy) PerkinElmer Optima 8300. The chemical elements detected were: Ca, S, K, Na, Mg, Li. The chloride identification was performed by conductimetry, pH & Ion-Meter GLP 2^2 from Crison, Chloride (Cl-) Ion Selective Electrode (*ISE*) from Hach.

2.2.2. X-ray diffraction (XRD)

Analysis of X-ray diffraction was performed on a X-ray diffractometer *PANalytical X'Pert PRO MPD θ/θ* powder diffractometer of 240 mm of radius, Cu Kα radiation (λ = 1.5418 Å); (45 kV – 40 mA); in a configuration of convergent beam with a focalizing mirror and a transmission geometry with flat samples sandwiched between low absorbing films; scan range: 2θ/θ from 4 to 88°2θ with a step size of 0.013°2θ and a measuring time of 300 s per step; Incident beam slits defining a beam height of 0.8 mm.; Incident and diffracted beam 0.04 rad *Soller* slits *PIXcel* detector: Active length = 3.347°. The powder sample was sandwiched between films of polyester, 3.6 μm thick. The Crystallographic phase identification was carried out using the X'pert HighScore PW3209 V2.2e software, and the identification of crystallographic phases was carried out using ICDD2000, PDF-2.

2.2.3. Scanning electron microscopy (SEM-EDX)

The analysis of particle morphology was carried out using a Jeol SEM equipment model JSM6360LV, coupled with an Inca Oxford EDS system. The measurements were carried out at a low vacuum, with a 20 kV electron beam, a working distance of 10 mm, a spot size of 60 mm, and a backscattered electron signal. For this same analysis, a Quanta 200 FEI SEM (XTE 325/D8395) coupled to an EDAX EDS system was also used. The measurements were carried out at a high vacuum and with an electron voltage of 20 kV, a working distance of 10 mm, and a backscattered electron signal.

2.3. Thermal behavior of carnallite

The thermal stability and reversible dehydration/hydration reaction of carnallite B were performed under different operating conditions as follows:

2.3.1. Dehydration reaction

The Dynamic dehydration of Carnallite B was measured using SDT-Q600 TA equipment with simultaneous TGA/DSC. The dynamic method used was from room temperature to 300 °C at a rate of 1 K/min. The nitrogen flow rate was set to 50.0 mL/min. For this analysis, 6.8 mg of sample was placed in a 90 μL platinum crucible with an unsealed lid to determine the change in weight and heat flow at high temperatures.

2.3.2. Determination of gaseous products by thermogravimetric-mass spectroscopy (TG-MS)

The gaseous products from Carnallite B dehydration at high temperatures were recorded by Thermogravimetric analysis (TG, SDTA 851e, Mettler Toledo) coupled to a mass spectrometer (MS, Pfeiffer Vacuum Thermostar). The measurements were performed from room temperature (25 °C) to 1100 °C, using dynamic experiments with a heating rate of 10 K/min. Nitrogen was used as the protective gas at a volume flow of 50 mL/min. The sample mass was surrounded by a constant nitrogen flow of 100 mL/min. A sample mass of about ~30 mg was measured in open Al_2O_3 crucibles.

2.3.3. Determination of solid products by High Temperature X-Ray Diffraction

The X-ray Diffraction patterns were measured at room temperature and at several temperatures: 50 °C,70 °C, 100 °C, 130 °C, 160 °C, 190 °C and 220 °C. with *PANalytical X'Pert PRO MPD θ/θ* powder diffractometer of 240 mm of radius, Cu Kα radiation (λ = 1.5418 Å), (45 kV–40 mA); in a configuration of convergent beam with a focalizing mirror and a transmission geometry with a spinner glass capillary sample holder. The scan range was from 10 to 80°2θ with a step size of 0.026°2θ and a measuring time of 160 s per step, the Incident and diffracted beam was 0.04 rad *Soller* slits and the *PIXcel* detector; Active length = 3.347° Oxford cryosystems 700 series Cryostream liquid nitrogen cryostat, enabling temperature control of the analyzed capillary sample from 90 to 500 °C. The material was analyzed in a Lindemann glass capillary with a diameter of 0.7 mm, opened at one end, using cooling and heating rates of 5 °C/min. The Crystallographic phase identification was carried

out using the X'pert HighScore PW3209 V2.2e software, and the identification of crystallographic phases was carried out using ICDD 2000, PDF-2.

2.4. Hydration reaction

2.4.1. STA–MHG reversibility of reaction

The reversibility of the reaction was carried out using a simultaneous thermal analyzer (NETZSCH STA 449 F3 Jupiter). Equipped with a differential scanning calorimetric and thermogravimetric (DSC-TG) sample holder with a thermocouple Type P and an accuracy of ±1 K, was used. The accuracy of the balance was ±0.1 μg. The equipment was coupled to a Modular Humidity Generator (ProUmid MHG-32). Nitrogen was used as a protective and purging gas with a volume flow of 20 mL/min for both purposes, and as the atmosphere surrounding the sample, keeping it inert by maintaining a nitrogen flow of 100 mL/min and excluding water vapor. Finally, liquid nitrogen was used to support the controlled cooling process, and the amount of sample mass used was ~10 mg in an open platinum crucible.

The chemical reversibility was calculated as a percentage of weight gained during hydration divided by the weight lost during dehydration, according to the following Eq. (4), where %R (reversibility), m_H = hydrated mass, m_D = Dehydrated mass, and m_0= initial mass.

$$\%R = \frac{m_H - m_D}{m_0 - m_D} \cdot 100 \tag{4}$$

The operating conditions, namely the temperature and humidity programs, used to evaluate the sample reversibility, were taken from [7] designed to evaluate the material for seasonal heat storage applications. They reproduce the partial pressure of water vapor and temperatures that are characteristic of summer and winter. These conditions should be suitable as indicated by the van't Hoff plot for synthetic carnallite [6,13] (Fig. 2). Hydration temperatures were set to 40 °C (corresponding to the minimum temperature for water heating), and dehydration temperatures were set to 110 °C (which can be easily reached by solar collector systems). The water vapor partial pressure conditions varied between 1.3 kPa (10.9% RH) and 4.0 kPa (35% RH) for the release and recovery of 4 mol of water (Eq. (2)).

2.4.2. Analysis of products after the hydration/dehydration cycles

Products obtained from the cycling experiments were analyzed at room temperature using XRD (PANalytical X'Pert Pro MPD, 45kVx40 mA; static air atmosphere, radiation of Cu Kα1 (λ = 1.5418 Å); Scan. Range: 10–80° in 2θ; Step Size: 0.013° and a measuring time of 75 s per step) to identify the phases of solid products that have been formed during hydrolysis reaction, which explains the material decomposition and the loss of reversibility.

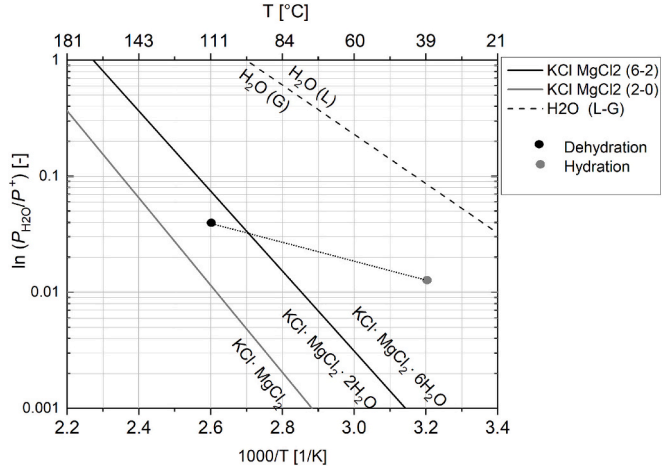

Fig. 2. Van't Hoff plot of $KCl{\cdot}MgCl_2{\cdot}6H_2O$ (Reproduced from [7] with permission). Equilibrium lines calculated under thermodynamic data ΔS = 150 J/mol·K [12] and ΔH = −66 kJ/mol (6–2) [13]. H_2O (g-l), ΔH = −40.65 kJ/mol, ΔS = 109.7 J/mol·K [12]. The H_2O(g)–H_2O(l) phase boundary is included solely as a reference for the water system and is not relevant for defining the stability limits of carnallite.

2.5. Energy storage density

The enthalpies of hydration and dehydration of the Carnallite B sample were obtained from differential scanning calorimetry (DSC) using the Software of the equipment (NETZSCH STA 449 F3 Jupiter) and NETZSCH-Proteus–Thermal Analysis, which integrates the specific power delivered to the samples (mW/mg) over time. The endothermic and exothermic behaviors were determined based on the tendencies of the DSC signal peaks (upwards or downwards, respectively) for 10 reaction cycles.

In addition, the amount of energy in Gigajoules (GJ) that can be stored in 1 m^3 (*esd*) was calculated as the product of the dehydration reaction enthalpy and density for the studied salt in its hydrated form (Eq. (5)), where $\Delta H_{(De)}$ is the reaction enthalpy (kJ/mol), M is the molar mass of the reactive compound ($KCl{\cdot}MgCl_2{\cdot}6H_2O$), and δ is the bulk density of the hydrated material.

$$esd = \frac{\Delta H_{(De)} \bullet \delta}{M} \tag{5}$$

The density of the solid sample was determined with a Helium pycnometer [24], using Accupyc 1330 V3. 03 equipment.

2.6. Application design

The reactor application was based on the energy density storage calculated from dehydration and hydration enthalpy of carnallite material, the volume (m^3) needed to store 8 GJ of energy, and respectively the amount of energy demanded to be used in a house (floor area of 110–120 m^2) [25,26].

3. Results and discussion

3.1. Chemical characterization

3.1.1. X-ray diffraction

In Fig. 3, the XRD pattern shows the presence of four main crystalline phases in the natural material: potassium carnallite ($KCl{\cdot}MgCl_2{\cdot}6H_2O$,

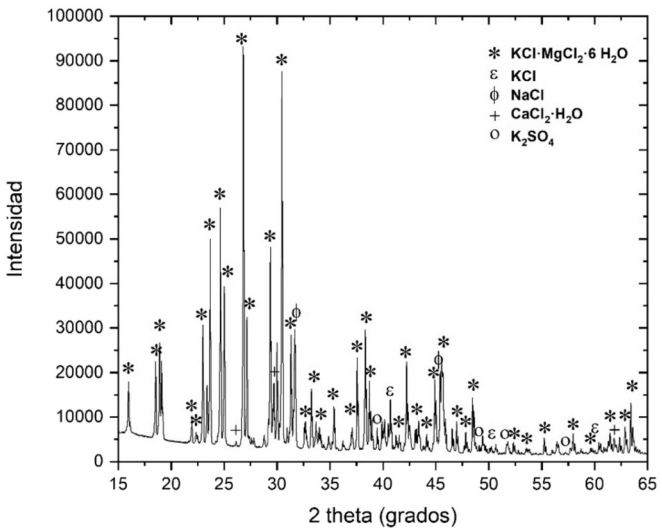

Fig. 3. XRD pattern of potassium carnallite B at 25 °C.

ref. code: 01-071-0727), silvite (KCl, ref. code: 000-04-0587), sodium chloride (NaCl, ref. code: 000-70-2509), and calcium chloride ($CaCl_2{\cdot}H_2O$, ref. code: 000-01-1104), minerals previously identified in the deposit of crystalline sea salts [8].

3.1.2. Chemical analysis

The identification of crystalline phases through XRD and elemental analysis via ICP-OES enabled the quantification of the concentration of each compound. The chemical elements found in carnallite are displayed in Table 2.

Analysis indicates that the material primarily consists of chloride, potassium, magnesium, and sodium, with trace amounts of calcium, sulfur, and lithium. Fig. 4 illustrates the mineral composition, revealing that potassium carnallite ($KCl{\cdot}MgCl_2{\cdot}6H_2O$) is the principal component, accounting for 86.0% by weight. The salt-based impurities include sodium chloride (10.2 wt%), potassium chloride (0.9 wt%), potassium sulfate (0.8 wt%), and calcium chloride monohydrated (2.0 wt%).

Additionally, since this material is extracted from natural sources, it exhibits a light pink color due to the presence of iron oxide impurities (less than 1%) [27], as well as inclusions of hematite and goethite, which are known to be part of the ore from which carnallite was mined [28].

Fig. 5 shows the morphology of the carnallite phase. Particles at 50× (Fig. 5A) close to 200 μm present an orthorhombic shape with no defined and linear edges. On the other hand, small particles look agglomerated on the bigger particles. NaCl is found on the surface of carnallite, like small cubic particles (Fig. 5B and C). Finally, the analysis in Fig. 5D, conducted via EDX, reveals the main elements Na, Mg, Cl, and K, which are also present in the chemical analysis. Notably, carnallite and NaCl are the primary impurities identified.

3.2. Dehydration reaction

3.2.1. Thermal stability

The dehydration of carnallite was studied through weight loss as the temperature was increased at controlled heating rates of 1 K/min. The thermal behavior is shown in two steps of weight loss (Fig. 6). It can be identified that the first step, the main endothermic dehydration, occurs between 57 and 118 °C, releasing 4.35 mol of H_2O (24.80 wt%), and the second step occurs between 118 and 150 °C, releasing 2.23 mol of H_2O (12.64 wt%). The total experimental mass loss observed was 34.68%, slightly up to 34.12% (theoretical dehydration). This would occur because an extra water adsorption takes place or a hydrolysis reaction releases HCl gas, as reported in previous work [7].

The energy involved in the first and second steps of dehydration was 778 kJ/kg and 327.5 kJ/kg, respectively.

The dehydration stages of carnallite B occur at a lower temperature than a synthetic carnallite material previously studied, where the step of dehydration takes place from 167 °C to 260 °C [12]. These differences between synthetic materials and a by-product sample are directly associated with the impurities present in each material. The impurities decrease the purity and increase the dehydration temperature of the active materials. In the case of synthetic carnallite, it contains 15.05% hexahydrated magnesium chloride, which is dehydrated together with the synthetic carnallite [12]. On the other hand, carnallite B has impurities that are not dehydrated in the thermal decomposition, so the mass loss corresponds only to the dehydration of carnallite.

Table 2
Carnallite B chemical analysis.

Elements	Composition, % *w*/w
Lithium, Li	<0.01
Sodium, Na	4.05
Potassium, K	14.23
Magnesium, Mg	8.48
Calcium, Ca	0.68
Chloride, Cl	44.73
Sulfur, S	0.20
H_2O	27.62

3.2.2. Determination of gaseous products by thermogravimetric – mass spectroscopy (TG-MS)

The release of HCl indicates the initiation of the hydrolysis reaction (Eq. (4)), which is irreversible and unfavorable for TCES applications. In Fig. 7, gas products were detected when carnallite was heated between 50 and 800 °C. In the analysis, a mass signal of 18 g/mol confirms the release of water in two dehydration steps in the temperature range of 80 to 210 °C. In addition, a weak mass signal of 36 g/mol is observed at high temperature and around 470 °C, indicating the release of HCl.

In comparison to other carnallite materials, decomposition occurs at a higher temperature, which poses challenges for its use as a thermochemical material [7]. This is because the hydrolysis reaction reduces reaction reversibility by gradually breaking down the material during cycles. Additionally, this reaction is highly corrosive to metals and toxic to human health. Therefore, for carnallite to be suitable as a thermochemical storage material, it is essential to limit its dehydration until just before the hydrolysis reaction begins.

3.2.3. Determination of solid products by HT-XRD

The analysis to determine the crystalline phases present during the dehydration process of the carnallite B sample was conducted using high-temperature X-ray diffraction, which was carried out at three different temperatures: 70 °C, 130 °C, and 160 °C. The XRD patterns obtained are shown in Fig. 8, where the broad baseline increase observed between 20° and 30° 2θ likely indicates the presence of a significant amorphous phase, which is typical for hydrated chloride salts after multiple dehydration/rehydration cycles at high temperatures [7].

The crystalline phases identified are detailed in Table 3. The results show that at 70 °C, the material has not been dehydrated, whereas at 130 °C, the material is dehydrated, forming $KCl{\cdot}MgCl_2{\cdot}2H_2O$ (ref. code: 00–001-0947), and four H_2O molecules are released. However, at 160 °C, $KCl{\cdot}MgCl_2$ (ref. code: 00–037-1408) and $Mg(OH)Cl$ (ref. code:00–003-0098) were identified, indicating the decomposition and an irreversible hydrolysis reaction product. Under these circumstances, the dehydration reaction should be set up to 130 °C to prevent the decomposition of carnallite.

3.3. Hydration reaction

To study carnallite B sample application as TCES, the optimal seasonal conditions were reproduced from previous optimized experiments using a by-product carnallite material (carnallite A) (experiment 6, Table 2) proposed by Mamani et al. [7]. The dehydration was carried out at 110 °C and a water pressure of 4.0 kPa. In contrast, the hydration was set at 40 °C and water pressure at 1.3 kPa for 6 h.

The results are shown in Fig. 9, where the dehydration/hydration reaction of carnallite B is observed over ten cycles. During the first cycle, the material presents a reversibility of 81.73%, which decreases to 78.83% in the tenth cycle. If these results are compared with those obtained for carnallite A and 73% of purity [7], It is observed that the reversibility of carnallite B is lower by 14% during the first cycle and 8.4% during the tenth cycle than the reversibility of carnallite A during the first and tenth cycles. However, carnallite B presents greater cyclic stability than carnallite A, with a loss of reversibility of 2.9% versus 8.5% for carnallite A during the tenth cycle.

The differences observed in the thermal behavior between the Carnallite A and Carnallite B samples can be attributed to variations in their impurities and their respective concentrations. In this case, Carnallite A contains 23.04% NaCl, while Carnallite B has 10.21%, with NaCl being the most abundant impurity in Carnallite A.

To better understand the cause of the thermal behavior of carnallite B material, these results were compared with the behavior of the synthetic material previously published by A. Gutiérrez et al., [12] And

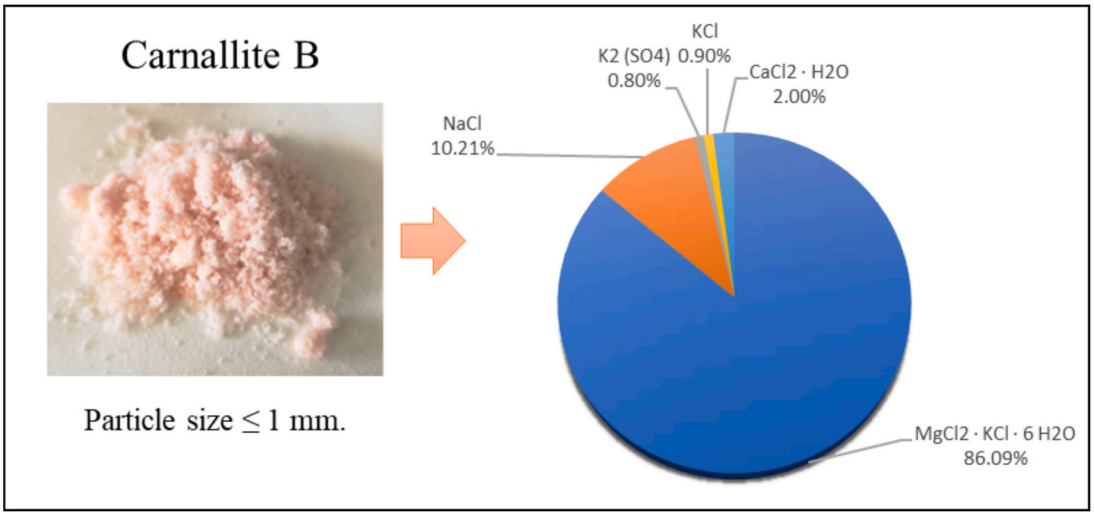

Fig. 4. Mineralization of potassium carnallite B.

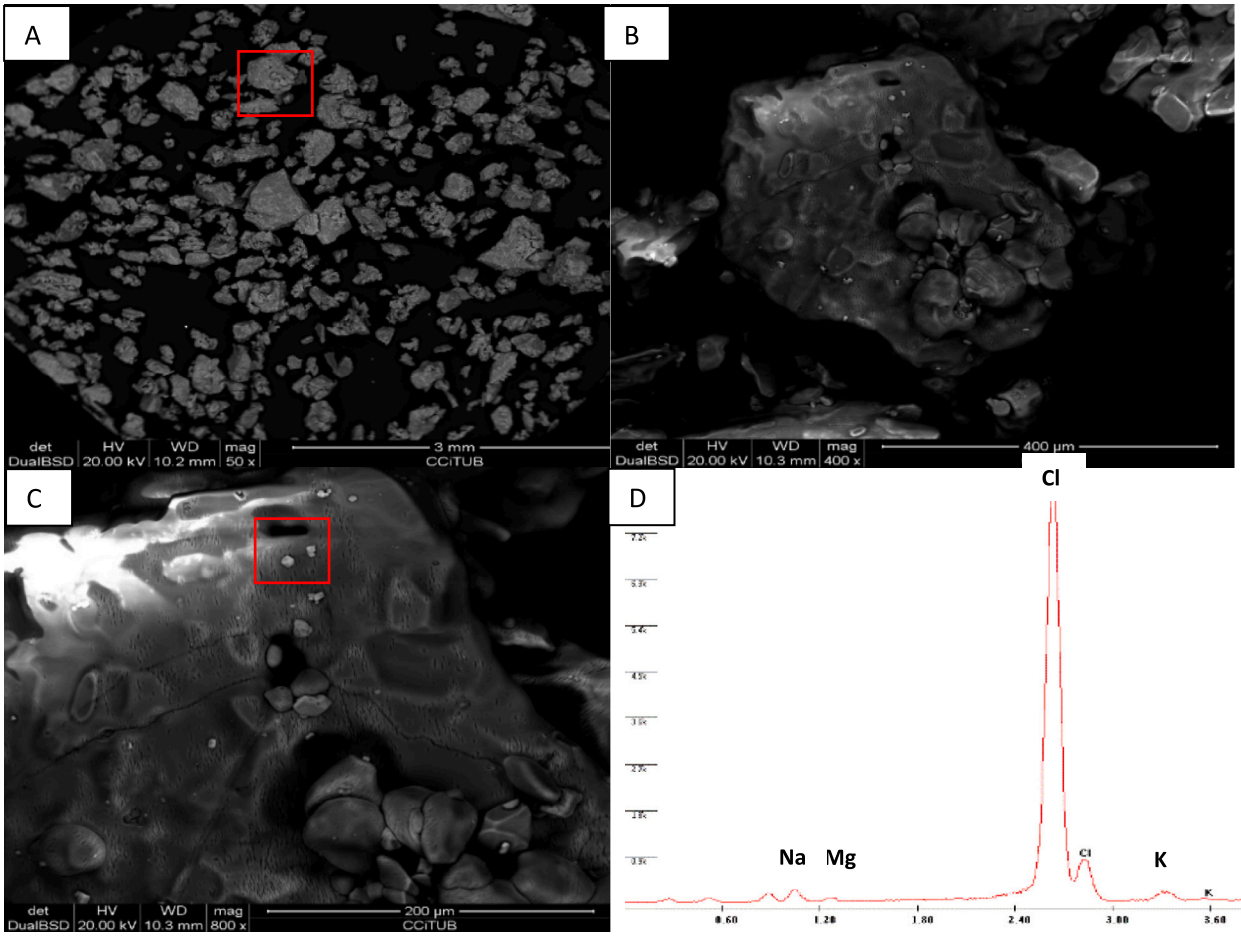

Fig. 5. Morphology of carnallite B particles using SEM-EDS. The images display different magnifications: A (50×), B (400×), C (800×), and D, which presents the energy-dispersive analysis of chemical elements.

subjected to the same experiment (see Fig. 10). In this analysis, synthetic carnallite (blue line) shows a reversibility of 45.65% during the first cycle, which is very low compared to carnallite A (green line) and carnallite B (black line). However, it is possible to observe that in the second cycle, the reversibility of carnallite B increases to 61.47% and remains stable, because during the tenth cycle, this reversibility decreases only by 1.37%. This being a carnallite synthetic that exhibits better cyclic stability during the 10-cycle reaction compared to the other carnallites, A and B.

The results indicate that carnallite B exhibits better reversibility compared to the synthetic material. This leads to the conclusion that the impurities (NaCl and KCl) present in both carnallite A and B enhance the

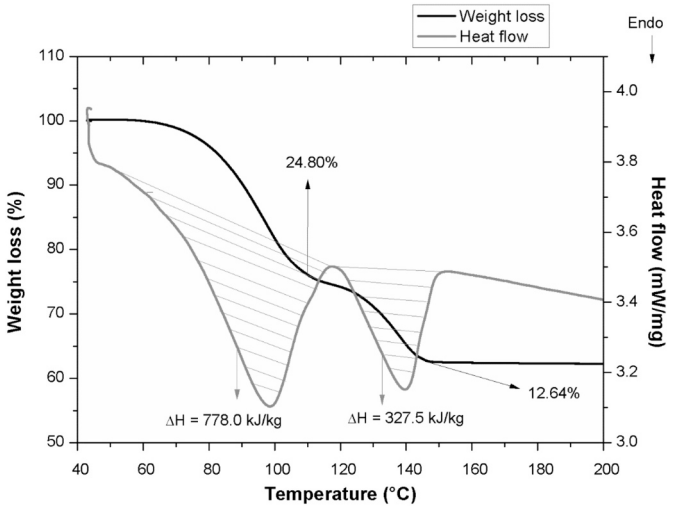

Fig. 6. TGA-DSC of carnallite B. Heat rate: 1 °C/min.

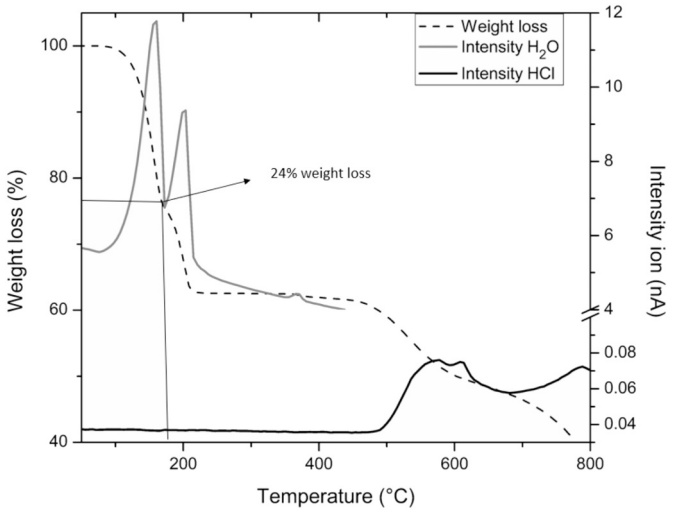

Fig. 7. TG-MS curve of thermal decomposition of carnallite B.

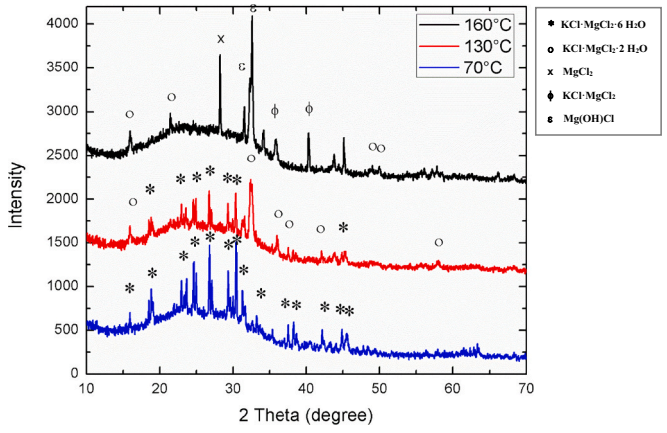

Fig. 8. Carnallite diffraction pattern at 70 °C, 130 °C, and 160 °C.

ability of carnallite particles to absorb a larger amount of water vapor, which in turn increases the percentage of reversibility and better hydration kinetics. Therefore, these impurities would serve as chemical spacing materials to mitigate the agglomeration effects. The observed

Table 3
Identification of products of carnallite thermal decomposition based on XRD at high temperature.

Solid products of the thermal decomposition of carnallite		
70 °C	130 °C	160 °C
$KCl{\cdot}MgCl_2{\cdot}6H_2O$	$KCl{\cdot}MgCl_2{\cdot}6H_2O$	$KCl{\cdot}MgCl_2{\cdot}2H_2O$
NaCl	$KCl{\cdot}MgCl_2{\cdot}2H_2O$	$KCl{\cdot}MgCl_2$
K_2SO_4	KCl	$MgCl_2$
$CaCl_2 \cdot H_2O$	K_2SO_4	$Mg(OH)Cl$
		K_2SO_4
		$CaCl_2$
		KCl

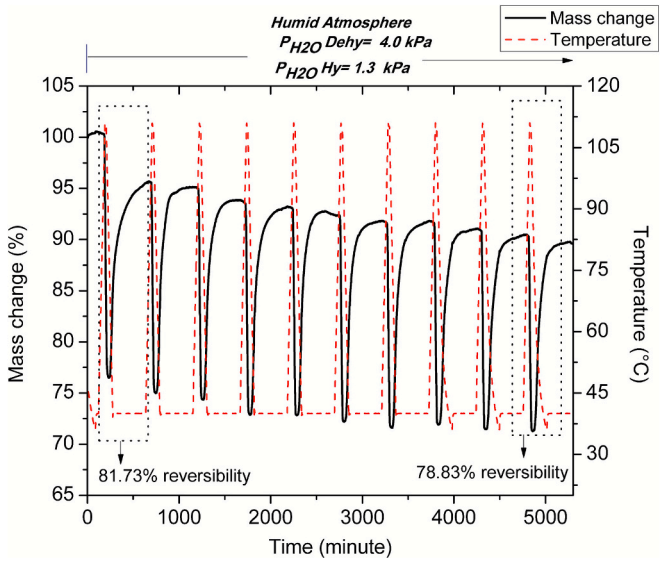

Fig. 9. Dehydration/hydration of carnallite B under seasonal conditions.

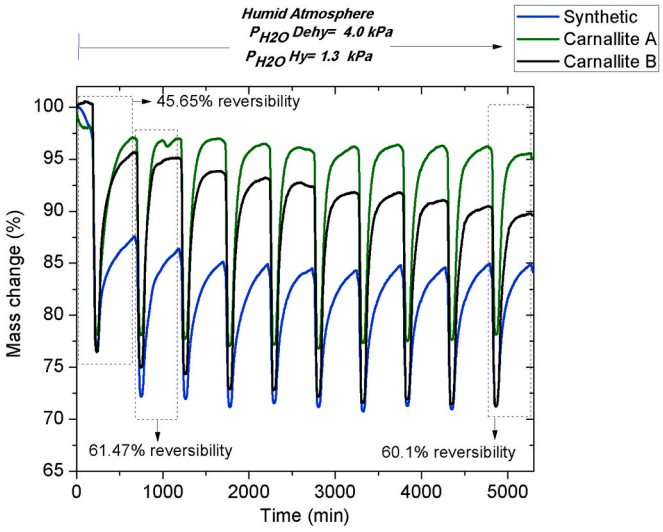

Fig. 10. Comparison of dehydration/hydration of carnallites under seasonal conditions.

decline in reversibility is most likely related to minor particle agglomeration, reduced porosity, or structural rearrangements occurring during repeated hydration–dehydration cycles. These mechanisms have been reported previously for chloride-based thermochemical materials [29] and can lead to increased mass transfer resistance.

Previous studies have demonstrated a positive effect of KCl in the

optimization of thermochemical materials, due to its high melting point [30]. NaCl would produce this same positive effect on the hydrated salts, as it has a melting point of 801 °C, which would improve the thermochemical qualities of carnallite A and B [31]. However, there are currently no studies that indicate an improvement in thermochemical materials made with NaCl mixtures.

3.4. Energy storage: density calculation

Thermochemical materials mixed with impurities (inactive materials), which do not participate in the reaction, decrease the energy density [11]. Due to this, the energy density of the dehydration/hydration reaction of carnallite was evaluated based on the enthalpy change (ΔH) during each cycle of the experiment (see Fig. 11). Based on these values and the density of carnallite B (1.6422 kg/m^3), obtained at 28.8 °C, the energy storage densities (*esd*) (GJ/m^3) were calculated like the amount of energy in gigajoules (GJ) stored in a volume of hydrated material of 1 m^3 for each dehydration stage (Table 4).

The results indicate that significant energy density values were obtained during the first four cycles of the hydration reaction of carnallite B. These values are comparable to the conditions previously described for seasonal heat storage materials [32]. Specifically, these conditions include a hydration energy density of 1.3 GJ/m^3 or higher, a hydration temperature of 50 °C, and a dehydration temperature below 120 °C. However, after the fourth cycle, energy density values decrease by up to 24% by the tenth cycle. This decline can be attributed to the reduced mass transfer during the hydration reaction, leading to decreased reversibility. To address this issue, one possible solution is to enhance energy storage density through doping with other materials to improve mass transfer. Alternatively, the material could be replaced every four years, which would not incur significant expenses since it is natural and abundant, thereby minimizing environmental impact.

Table 3 also presents the *esd* of carnallite A, as previously reported by Mamani et al. [7]. By comparing these data, we can determine that the hydration energy densities of carnallite A are approximately 10% higher than those of carnallite B. This difference is attributed to the lower reversibility of carnallite B, meaning that less material is involved in the reaction. Consequently, carnallite A is a more favorable material for reuse in home heating applications compared to carnallite B.

The values of *esd* estimated based on hydration enthalpy were directly correlated with the material volume needed to store 8 GJ of energy, considered the required energy capacity to supply the heat

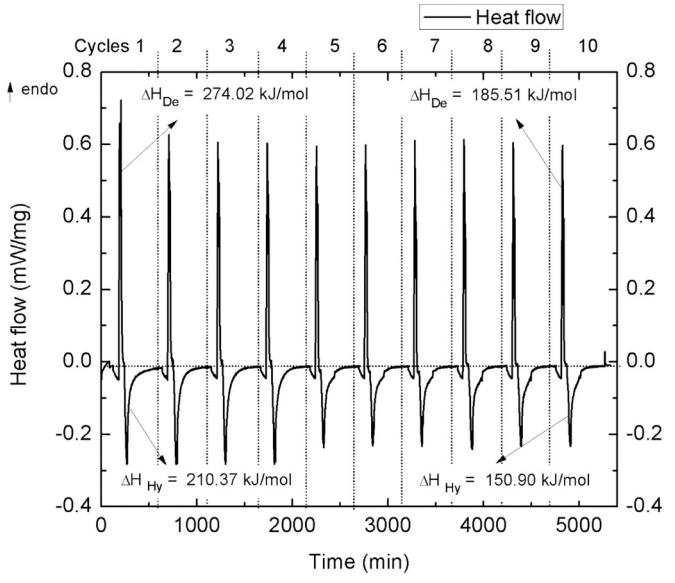

Fig. 11. Enthalpies of dehydration/hydration from the experiment of 10 cycles.

Table 4
Energy storage density estimated for dynamic dehydration of carnallite B. Hydration energy storage density ***(esd(Hy))*** is calculated using the absolute value of the hydration enthalpy ***(–ΔH(Hy))***.

M: 277.6 g/mol		ρ[28.8 °C] = 1.6422 g/cm^3			
Cycles	*ΔH(De)* [kJ/mol]	*Esd (De)* [GJ/m^3]	*ΔH(Hy)* [kJ/mol]	*esd(Hy)*[GJ/m^3] Carnallite B	*esd(Hy)*[GJ/m^3][a] [7] Carnallite A
1	274.02	1.621	−210.37	1.244	1.417
2	237.27	1.403	−207.33	1.226	1.413
3	234.23	1.385	−203.54	1.204	1.453
4	214.98	1.271	−202.16	1.195	1.414
5	206.75	1.223	−178.69	1.057	1.243
6	201.58	1.192	−188.88	1.117	1.202
7	198.09	1.171	−154.37	0.913	1.210
8	193.58	1.145	−153.94	0.910	1.114
9	189.81	1.122	−156.83	0.927	1.127
10	185.51	1.097	−150.90	0.892	1.129

[a] Energy storage density calculated for carnallite A in a previous article published by Mamani and co-workers [7].

demands of a typical house during the cold seasons. This value was calculated using an average of *esd* of 1.0685 GJ/m^3. The computed volume was 7.5 m^3 and a mass of 12,316 kg (Fig. 12), representing a considerable area and amount of material that is not directly applicable to real-scale residential systems. Therefore, it is essential to enhance the energy storage by improving mass transfer and ensuring that the active materials remain engaged in the reaction.

Regarding the energy storage cost, when normalized per unit of energy stored, this corresponds to approximately 0.25 €/GJ for carnallite compared to >160 €/GJ for $MgCl_2$ systems [33]. This significant cost advantage reinforces the potential of natural carnallite as a low-cost thermochemical material for large-scale seasonal energy storage.

Additionally, the study aimed to evaluate the natural carnallite inherent energy storage potential at a laboratory level, establishing a foundation for future system design. The next step involves researching reactor technologies for carnallite to facilitate scaling up these applications. In practical use, however, the material would need to be processed into structured forms (e.g., pellets, granules, or composites) to enhance volumetric energy density, heat and mass transfer, and mechanical strength.

4. Conclusions

This study presents a complementary investigation on Carnallite B, a potash mining by-product from the Spanish industry characterized by a distinct chemical profile (86.09% $KCl{\cdot}MgCl_2{\cdot}6H_2O$, 10.21% NaCl, 2.00% $CaCl_2{\cdot}H_2O$, 0.90% KCl, and 0.80% K_2SO_4). The material was chemically and thermally characterized under controlled seasonal operating conditions to enable a direct comparison with a by-product carnallite from the Chilean industry, previously reported, providing new insights into the role of impurities in thermochemical energy storage performance.

The conditions for hydration were P_{Hy} = 1.3 kPa and T_{Hy} = 40 °C, while those for dehydration were P_{De} = 4.0 kPa and T_{De} = 110 °C. In the first cycle, the material shows a reversibility of 81.73%, which decreases to 78.83% by the tenth cycle. When comparing these results to those obtained for carnallite A with 73% purity, it is noted that the reversibility of carnallite B is lower by 14% in the first cycle and by 8.4% in the tenth cycle. However, carnallite B demonstrates greater cyclic stability than carnallite A, with a loss of reversibility of 2.9% compared to 8.5% loss for carnallite A in the tenth cycle.

The differences in thermal behavior between carnallite B and carnallite A can be attributed to variations in the types and concentrations of impurities present. Notably, NaCl is the impurity found in the highest concentration in previously reported carnallite A. This argument

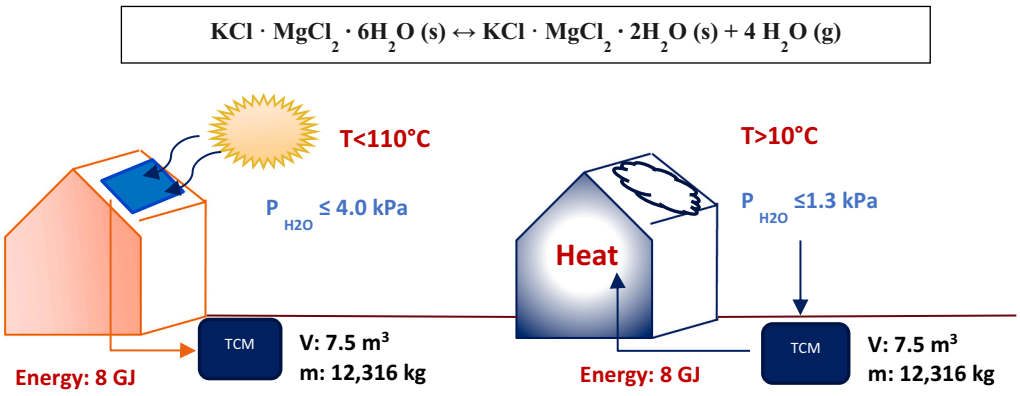

Fig. 12. Representation of seasonal thermochemical storage application using carnallite B.

was validated by comparing it with a synthetic carnallite, which, under the same seasonal conditions, exhibits a low reversibility of 45.65% during the first cycle and slow hydration kinetics. However, further experiments mixing synthetic carnallite with different concentrations of impurities are necessary to conclude the real effect of NaCl and KCl present in both carnallite A and B on enhancing the ability of carnallite particles to absorb a larger amount of water vapor, which in turn increases the percentage of reversibility and improves hydration kinetics.

Furthermore, HT-XRD and TG-MS analysis indicated that the loss of reversibility may not be attributed to hydrolytic decomposition, but rather to the crystalline properties of the particles and a decrease in mass transfer during hydration.

Regarding the energy storage density values, the volume and mass of material needed to store 8 GJ of energy, which is the amount required to supply the heat needs of a typical home in the winter season, would be 7.5 m^3 and 12,316 Kg, respectively, for a system using carnallite B as a material. This poses a challenge in space and building construction, as it would require a large area to store the reactor. Therefore, it is crucial to enhance energy storage by improving mass transfer during hydration reactions, involving more material for the response, and studying reactor technologies.

In general, carnallite B presents several advantages over other TCM, primarily due to its low cost as an abundant product of seawater evaporation. Its composition, which includes KCl and NaCl, results in lower hygroscopicity, and utilizing carnallite B could enhance the viability of thermochemical applications and promote sustainable energy practices.

CRediT authorship contribution statement

V. Mamani: Writing – original draft, Investigation, Data curation, Conceptualization. **A. Gutiérrez:** Writing – review & editing, Methodology, Formal analysis. **A.I. Fernández:** Writing – review & editing, Resources, Methodology, Funding acquisition, Conceptualization. **S. Ushak:** Writing – review & editing, Supervision, Investigation, Funding acquisition, Formal analysis, Conceptualization.

Declaration of competing interest

The authors declare the following financial interests/personal relationships which may be considered as potential competing interests: Fernandez, A.I. reports financial support was provided by Spain Ministry of Science and Innovation. Mamani, V. reports financial support was provided by National Agency for Research and Development. Ushak, S. reports was provided by National Agency for Research and Development. Fernandez, A.I. reports administrative support was provided by Government of Catalonia Agency for Administration of University and Research Grants. Given her role as Associate Editor, the co-author Svetlana Ushak had no involvement in the peer review of this article and had no access to information regarding its peer review. Full responsibility for the editorial process for this article was delegated to another journal editor. If there are other authors, they declare that they have no known competing financial interests or personal relationships that could have appeared to influence the work reported in this paper.

Acknowledgements

Verónica Mamani thanks CONICYT for her doctorate scholarship CONICYT No. 21150145, Svetlana Ushak thanks the financial support of ANID/PUENTE N° 1523A0006, ANID/FONDECYT REGULAR N° 1231721, and CONICYT/PCI/REDES N°170131 projects. Andrea Gutierrez would like to thank DAAD for her DLR/DAAD Postdoctoral fellowship.

The University of Barcelona and the Diopma group thank the Grant PID2021-123511OB-C32, funded by MCIU/AEI/10.13039/501100011033 and by FEDER, UE, and the Catalan Government, for the quality accreditation (2021SGR708).

Data availability

Data will be made available on request.

References

[1] Energy consumption in households - Statistics Explained, (n.d.). https://ec.europa.eu/eurostat/statistics-explained/index.php?title=Energy_consumption_in_households (accessed March 18, 2025).
[2] The European Green Deal - European Commission, (n.d.). https://commission.europa.eu/strategy-and-policy/priorities-2019-2024/european-green-deal_en (accessed March 18, 2025).
[3] M. Luberti, R. Gowans, P. Finn, G. Santori, An estimate of the ultralow waste heat available in the European Union, Energy 238 (2022) 121967, https://doi.org/10.1016/J.ENERGY.2021.121967.
[4] J. Stengler, M. Linder, Thermal energy storage combined with a temperature boost: An underestimated feature of thermochemical systems, Appl. Energy 262 (2020), https://doi.org/10.1016/j.apenergy.2020.114530.
[5] Wim van Helden, Task 67-Compact Thermal Energy Storage Materials Within Components Within Systems THE ISSUE, 2023.
[6] T. Yang, W. Liu, G.J. Kramer, Q. Sun, Seasonal thermal energy storage: a techno-economic literature review, Renew. Sust. Energ. Rev. 139 (2021), https://doi.org/10.1016/j.rser.2021.110732.
[7] V. Mamani, A. Gutiérrez, A.I. Fernández, S. Ushak, Industrial carnallite-waste for thermochemical energy storage application, Appl. Energy 265 (2020), https://doi.org/10.1016/j.apenergy.2020.114738.
[8] I. Ihsanullah, J. Mustafa, A.M. Zafar, M. Obaid, M.A. Atieh, N. Ghaffour, Waste to wealth: a critical analysis of resource recovery from desalination brine, Desalination 543 (2022), https://doi.org/10.1016/j.desal.2022.116093.
[9] W. Hua, H. Yan, X. Zhang, X. Xu, L. Zhang, Y. Shi, Review of salt hydrates-based thermochemical adsorption thermal storage technologies, J. Energy Storage 56 (2022), https://doi.org/10.1016/j.est.2022.106158.
[10] A. Gutierrez, S. Ushak, V. Mamani, P. Vargas, C. Barreneche, L.F. Cabeza, M. Grágeda, Characterization of wastes based on inorganic double salt hydrates as potential thermal energy storage materials, Sol. Energy Mater. Sol. Cells 170 (2017) 149–159, https://doi.org/10.1016/j.solmat.2017.05.036.

[11] H.U. Rammelberg, T. Osterland, B. Priehs, O. Opel, W.K.L. Ruck, Thermochemical heat storage materials – performance of mixed salt hydrates, Sol. Energy 136 (2016) 571–589, https://doi.org/10.1016/j.solener.2016.07.016.
[12] A. Gutierrez, S. Ushak, M. Linder, High carnallite-bearing material for thermochemical energy storage: thermophysical characterization, ACS Sustain. Chem. Eng. 6 (2018) 6135–6145, https://doi.org/10.1021/acssuschemeng.7b04803.
[13] R. Hamze, I. Nevoigt, U. Sazama, M. Fröba, M. Steiger, Carnallite double salt for thermochemical heat storage, J. Energy Storage 86 (2024), https://doi.org/10.1016/j.est.2024.111404.
[14] M. Molenda, J. Stengler, M. Linder, A. Wörner, Reversible hydration behavior of CaCl2 at high H2O partial pressures for thermochemical energy storage, Thermochim. Acta 560 (2013) 76–81, https://doi.org/10.1016/j.tca.2013.03.020.
[15] P.A.J. Donkers, L. Pel, O.C.G. Adan, Experimental studies for the cyclability of salt hydrates for thermochemical heat storage, J. Energy Storage 5 (2016) 25–32, https://doi.org/10.1016/j.est.2015.11.005.
[16] P.J. Masset, Thermogravimetric study of the dehydration reaction of LiCl•H 2O, J. Therm. Anal. Calorim. 96 (2009) 439–441, https://doi.org/10.1007/s10973-008-9399-y.
[17] G. Yang, M. Ji, Y. Huang, X. She, Y. Luo, L. Wang, L. Wang, Characterization and performance analysis of SrCl2 impregnated activated alumina composites for solar thermal energy storage, Sol. Energy Mater. Sol. Cells 282 (2025), https://doi.org/10.1016/j.solmat.2024.113385.
[18] V.M. Van Essen, H.A. Zondag, J. Cot Gores, L.P.J. Bleijendaal, M. Bakker, R. Schuitema, W.G.J. Van Helden, Z. He, C.C.M. Rindt, Characterization of MgSO4 hydrate for thermochemical seasonal heat storage, J. Solar Energ. Eng. Trans. ASME 131 (2009) 0410141–0410147, https://doi.org/10.1115/1.4000275.
[19] K.E. N'Tsoukpoe, H. Liu, N. Le Pierrès, L. Luo, A review on long-term sorption solar energy storage, Renew. Sust. Energ. Rev. 13 (2009) 2385–2396, https://doi.org/10.1016/j.rser.2009.05.008.
[20] T.R.S. Gbenou, K. Wang, Kinetic analysis of poly-aluminum sulfate hydrate for low-temperature thermochemical heat storage, Appl. Therm. Eng. 210 (2022), https://doi.org/10.1016/j.applthermaleng.2022.118317.
[21] J. Stengler, J. Weiss, M. Linder, Analysis of a lab-scale heat transformation demonstrator based on a gas–solid reaction †, Energies (Basel) 12 (2019) https://doi.org/10.3390/en12122234.
[22] K.E. N'Tsoukpoe, N. Le Pierrès, L. Luo, Experimentation of a LiBr-H2O absorption process for long-term solar thermal storage: Prototype design and first results, Energy 53 (2013) 179–198, https://doi.org/10.1016/j.energy.2013.02.023.
[23] S. Ushak, A. Gutierrez, E. Flores, H. Galleguillos, M. Grageda, Development of thermal energy storage materials from waste-process salts, in: Energy Procedia, Elsevier Ltd, 2014, pp. 627–632, https://doi.org/10.1016/j.egypro.2014.10.217.
[24] A. Minevich, Y. Marcus, L. Ben-Dor, Densities of solid and molten salt hydrates and their mixtures and viscosities of the molten salts, J. Chem. Eng. Data 49 (2004) 1451–1455, https://doi.org/10.1021/je049849b.
[25] C.J. Ferchaud, H.A. Zondag, A. Rubino, R. De Boer, Seasonal Sorption Heat Storage-Research on Thermochemical Materials and Storage Performance ECN-M–12-070, 2012.
[26] N. Patricia, R. Ramos, P. Guía, G. Rodriguez, J.M. De, L.A. Comisión, M. Bustamante, S. Mauricio, T. Villegas, S. De Chile, Universidad de Chile Facultad de Ciencias Físicas y Matemáticas Departamento de Ingeniería Civil consumo de energía a nivel residencial en Chile y análisis de eficiencia energética en calefacción memoria para optar al título de ingeniero civil, 2011.
[27] La mineria de potassa al Bages: informe de l'Estudi Ramon Folch i s'Altesa Reial el Príncep d'Astúries cancel·la la visita anunciada a Iberpotash-Súria, Notícies de La ICHN n.105 (2013).
[28] P. Laura, R. Ortiz, J. Jos, P. Mur, Características geoquímicas de la formación de sales potásicas de Navarra (Eoceno superior). Comparación con la cuenca potásica catalana (l), Acta Geol. Hisp. 19 (2) (1984) 81–95.
[29] E. Barbosa, A.K. Menon, Thermochemical energy storage using salt mixtures with improved hydration kinetics and cycling stability, J. Energy Storage 90 (2024), https://doi.org/10.1016/j.est.2024.111916.
[30] K. Korhammer, M.M. Druske, A. Fopah-Lele, H.U. Rammelberg, N. Wegscheider, O. Opel, T. Osterland, W. Ruck, Sorption and thermal characterization of composite materials based on chlorides for thermal energy storage, Appl. Energy 162 (2016) 1462–1472, https://doi.org/10.1016/j.apenergy.2015.08.037.
[31] A. Shkatulov, Y. Aristov, Modification of magnesium and calcium hydroxides with salts: An efficient way to advanced materials for storage of middle-temperature heat, Energy 85 (2015) 667–676, https://doi.org/10.1016/j.energy.2015.04.004.
[32] P.A.J. Donkers, L.C. Sögütoglu, H.P. Huinink, H.R. Fischer, O.C.G. Adan, A review of salt hydrates for seasonal heat storage in domestic applications, Appl. Energy 199 (2017) 45–68, https://doi.org/10.1016/j.apenergy.2017.04.080.
[33] V. Mamani, A. Gutiérrez, S. Ushak, Development of low-cost inorganic salt hydrate as a thermochemical energy storage material, Sol. Energy Mater. Sol. Cells 176 (2018) 346–356, https://doi.org/10.1016/j.solmat.2017.10.021.